Adaptive Terminal Sliding Mode Control for Asteroid Hovering by Solar Sailing: Application to 433 Eros

Zitong Lin[a,**], Matteo Ceriotti[a], Colin R. McInnes[a]

[a]*James Watt School of Engineering, University of Glasgow, Glasgow, United Kingdom*

Abstract

In this paper, we propose a second-order sliding mode control law of solar sail to hover on displaced orbits above an asteroid. To overcome the difficulties of solar sail control, firstly, dynamics in cylindrical coordinates are used and only the hovering radii and height are controlled, neglecting the polar angle; secondly, the angular velocity of two attitude angles is taken as the control input instead of the angles themselves; lastly, an adaptive estimation law is applied to increase the robustness to gravity uncertainty. The case of hovering on displaced orbits above 433 Eros is simulated. The effect of different hovering radius, height and sunlight incidence direction are studied. In addition, the robustness of the control law is tested against unknown gravity disturbances and imprecise sail force model. This work successfully demonstrates that it is feasible to achieve an asteroid-hovering mission using an underactuated solar sail with only two controllable attitude angles.

Keywords: Underactuated solar sail, asteroid hovering orbit, second-order sliding mode control, adaptive estimation

1. Introduction

Asteroids, a type of small bodies, are widely-distributed living fossils in the solar system. As the space exploration deepens, these inconspicuous space rocks have attracted more attention of researchers and space agencies around the world. Asteroid exploration not only helps to reveal the origin of solar system, but it also assists significantly with space resource exploitation and planetary defence. There have been many representative examples of asteroid missions. In 2001, NEAR-Shoemaker probe to 433 Eros had become the first one to orbit and land on an asteroid [1]. The Hayabusa mission to 25143 Itokawa had achieved sample return of an asteroid for the first time in 2010 [2]. The follow-up Hayabusa 2 mission to 162173 Ryugu made multiple surface interactions with MASCOT landers, as well as performing a sample return [2]. These missions have brought many successes, not only in better knowing of asteroid physical properties, but also in boosting technologies in deep space exploration.

Since transfers to asteroids usually require high delta-v budgets, solar sailing can be an ideal option as it is capable of providing a theoretically-unlimited delta-v. Extensive research has investigated the use of solar sails for asteroid rendezvous missions [3-5], while little effort has been made on the operations of a solar sail in close proximity of an asteroid. In order to maximise the scientific return of the mission, asteroid flying-by reconnaissance is not enough and close-proximity operations will be essential, including hovering.

Hovering is a practical option of mapping an asteroid: the spacecraft flies on the displaced orbit above a certain region of the asteroid or keep stationary at a certain location, which therefore takes advantage in high-resolution imaging [6], landing [7], lander deployment [8] and sampling [2]. However, hovering above an asteroid is energy-consuming as it seeks no benefit from natural motion in most cases, making it only suitable for asteroids of small dimension [9]. Regarding this issue, solar sailing may offer a possible solution to hovering above large asteroids because of the continuous propellant-free acceleration.

New concepts of spacecraft in asteroid missions bring new challenges in control. Firstly, differently from spacecraft with three-axis thrust, a conventional sail-craft only has two control variables, namely attitude angles, for orbit control, resulting in an acceleration vector that is constrained in both direction and magnitude. Thus, it is challenging or impossible to track any arbitrary orbit in three dimensions; this is indeed typical of an underactuated system. Secondly, the input sail attitude angles affect its dynamics via trigonometric

* Corresponding author email, z.lin.1@research.gla.ac.uk

terms; in other words, the control is not linear and non-affine. An additional complexity is that the gravity field of an asteroid is highly irregular and cannot be precisely known prior to a mission, adding uncertainty and disturbances to the control problem.

Yet some research provides insights in the control of solar sail in proximity of asteroids. Biggs and McInnes [10] proposed the Time-Delayed Feedback Control (TDFC) as a method of bounding the orbit of a spacecraft around a central body with large ellipticity. Rather than depending on some reference trajectory, this method uses the state known one period previous to the current state as the reference. Farrés et al. [11-13] have studied a series of work on the dynamics of solar sail near an asteroid. These works brilliantly inherited the complete theory of linear control and orbit dynamics in CR3BP, but the linearisation involved cannot guarantee global stability, which means stable controlled orbits can be designed only near the equilibrium points. Zeng [14] considered the solar sail with controllable reflectivity and globally searched the feasible hovering regions above an asteroid with sunlight incident direction taken into account. The reflectivity change is the third control that complements the attitude manoeuvres to solve the underactuated problem, but it will significantly increase the system complexity and cost. Moore and Ceriotti [15] proposed the Genetic Algorithm and Control Transition Matrix (GA & CTM) method and found its application in eliminating the non-spherical gravity perturbation of an asteroid on solar sail orbits. This method uses an optimisation approach to obtain the control so that non-affine and underactuated problems are avoided. However, due to the black-box nature of GA, the desired orbit can only be selected within unforeseeable candidates but cannot be predefined arbitrarily, especially in terms of non-Keplerian orbits above asteroids. In addition, the sliding mode control (SMC), a control strategy robust to disturbances, attracts as much attention for its wide application in spacecraft orbit control. There has been research about asteroid landing [7] and orbiting [16, 17] missions with SMC; in this paper, its application in the orbit control of solar sail will be investigated.

In this paper, an adaptive terminal sliding mode control is proposed for the hovering control close to asteroid Eros. A displaced (non-Keplerian) circular orbit is selected as reference, and by converting the dynamics from Cartesian to cylindrical coordinates, the desired displaced orbit radius and hovering height are tracked regardless of polar angle, which transforms the underactuated system into a fully-actuated one. By differentiating the dynamics, the first-order derivatives of the sail attitude angles appear in linear form and are therefore chosen as the control input so that the non-affine issue can be solved. Moreover, an estimation law is designed to update the upper bound of disturbances, making the control robust to the complex gravity field of an asteroid.

2. Dynamics

2.1. Frames of Reference

A sketch of the reference frames is shown in Fig. 1. The first frame is the principal axis frame fixed with the asteroid referred to as $Oxyz$ (denoted as frame a). It is centred at the barycentre of the asteroid and it rotates about z axis defined by the constant self-spin rate of the asteroid, $\boldsymbol{\omega} = \omega\hat{\boldsymbol{z}}$ (the hat above a vector is used throughout this paper to indicate its unit vector) where ω is the modulus of angular velocity. x axis lies in the equatorial plane normal to z axis and y axis completes the triad. The inertially-fixed frame $OXYZ$ (which is not shown in Fig. 1 and denoted as frame I) coincides with $Oxyz$ at the initial time. If only a short time of flight around the asteroid is considered, it is reasonable to take this frame as fixed with respect to the sun direction, because the asteroid spin period (in the order of hours) is negligible with respect to its orbital period (in the order of years). Another important frame is the light incidence frame $Oe_xe_ye_z$ (denoted as frame E). e_z is aligned with the solar incident direction, e_y coincides with Y axis and e_x completes the triad. The relative position between the Sun and the asteroid can be described by the solar incidence angle $\varphi \in [-\pi/2, \pi/2]$, defined as the angle between e_z axis and Z axis. The last frame is the hovering orbit frame $ox_hy_hz_h$ (denoted as frame h). The ox_hy_h plane lies in the hovering plane which is perpendicular to the z axis and x_h, y_h, z_h axes follow the directions of outward radial, forward tangential and upward respectively.

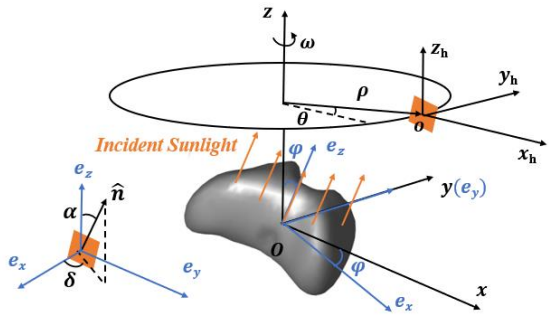

Fig. 1. Diagram of asteroid-fixed frame, light incidence frame, hovering orbit frame and solar sail attitude angles.

The coordinate transformations among the different frames are shown below:

$$E \xrightarrow{\mathbf{C}_y(\varphi)} I \xrightarrow{\mathbf{C}_z(\omega t)} a \xrightarrow{\mathbf{C}_z(\theta)} h \tag{1}$$

where the rotation matrices are:

$$\mathbf{C}_E^I = \begin{bmatrix} \cos\varphi & 0 & -\sin\varphi \\ 0 & 1 & 0 \\ \sin\varphi & 0 & \cos\varphi \end{bmatrix} \quad (2)$$

$$\mathbf{C}_I^h = \begin{bmatrix} \cos(\theta+\omega t) & \sin(\theta+\omega t) & 0 \\ -\sin(\theta+\omega t) & \cos(\theta+\omega t) & 0 \\ 0 & 0 & 1 \end{bmatrix} \quad (3)$$

$$\mathbf{C}_a^h = \begin{bmatrix} \cos\theta & \sin\theta & 0 \\ -\sin\theta & \cos\theta & 0 \\ 0 & 0 & 1 \end{bmatrix} \quad (4)$$

2.2. Model of Asteroid Gravity

Polyhedron method is one of the methods to model the gravitational field of an asteroid while reflecting the perturbation induced by its irregular shape. The gravity potential in asteroid-fixed frame can be written as:

$$U = -G\rho \sum_{e\in edges} \mathbf{E}_e \boldsymbol{r}_e L_e + G\rho \sum_{f\in faces} \mathbf{F}_f \boldsymbol{r}_f \omega_f \quad (5)$$

where G is the gravitational constant and ρ is the constant density of the asteroid. As can be seen, this expression is made up of two different contributions: the first is associated with the edges of each face and the second with the faces of each tetrahedron which form the surface of the body. The term $\boldsymbol{r}_e$ represents a vector from a field point to any point on the edge e, while the term $\boldsymbol{r}_f$ represents a vector from a field point to any point on the face f. $\mathbf{E}_e$ and $\mathbf{F}_f$ are two tensors: the first takes into account the geometry of the edges and the second considers the geometry and the orientation of the faces. Finally, L_e and ω_f are two scalars: the first is the potential of a 1D straight wire and ω_f is the signed solid angle subtended by the face f. Further details about calculation can be referred to the work of Werner and Scheeres [18].

2.3. Model of Solar Sail

Consider an ideal solar sail, the solar radiation pressure (SRP) acceleration can be modelled as [19]:

$$\boldsymbol{a}_{SRP} = a_0 \cos^2\alpha\, \hat{\boldsymbol{n}} \quad (6)$$

where a_0 is the constant part in SRP acceleration determined by the lightness number β, the solar gravitational constant μ_s and heliocentric distance R.

$$a_0 = \frac{\beta\mu_s}{R^2} \quad (7)$$

$\hat{\boldsymbol{n}}$ is the unit vector of sail normal in light incidence frame, expressed as:

$$\hat{\boldsymbol{n}} = [\sin\alpha\cos\delta \quad \sin\alpha\sin\delta \quad \cos\alpha]^T \quad (8)$$

where $\alpha \in [0, \pi/2]$ is the cone angle, defined as the angle between $\hat{\boldsymbol{n}}$ and e_z axis, and δ is the clock angle, defined as the angle between e_x axis and the projection of $\hat{\boldsymbol{n}}$ on Oe_xe_y plane (see Fig. 1).

2.4. Dynamics in Cylindrical Coordinates

Similar to the work on SRP geocentric displaced orbit in Ref. [20, 21], dynamics in cylindrical coordinates is adopted in order to facilitate the design. The dynamics of a solar sail at position $\boldsymbol{r} = [x, y, z]^T$ in asteroid-fixed frame a is given by:

$$\ddot{\boldsymbol{r}} + 2\boldsymbol{\omega}\times\dot{\boldsymbol{r}} + \boldsymbol{\omega}\times(\boldsymbol{\omega}\times\boldsymbol{r}) = \boldsymbol{\nabla}U + \boldsymbol{f}_{SRP} \quad (9)$$

where $\boldsymbol{\nabla}U$ is the gradient of gravity potential and $\boldsymbol{f}_{SRP}$ is the SRP acceleration in asteroid-fixed frame.

By substituting $x = \rho\cos\theta$ and $y = \rho\sin\theta$, the dynamics in Cartesian coordinates can be converted into the cylindrical coordinates (ρ, θ, z) shown below:

$$\begin{cases} \ddot{\rho} = \rho(\omega+\dot{\theta})^2 + g_\rho + f_\rho \\ \rho\ddot{\theta} = -2\dot{\rho}(\omega+\dot{\theta}) + g_\theta + f_\theta \\ \ddot{z} = g_z + f_z \end{cases} \quad (10)$$

where

$$\boldsymbol{g} = [g_\rho, g_\theta, g_z]^T = \mathbf{C}_a^h \boldsymbol{\nabla}U \quad (11)$$

$$\boldsymbol{f} = [f_\rho, f_\theta, f_z]^T = \mathbf{C}_I^h \mathbf{C}_E^I \boldsymbol{a}_{SRP} \quad (12)$$

In the next chapter, $\boldsymbol{f}$, the SRP acceleration in hovering orbit frame h, is to be controlled so that the solar sail can hover on the displaced orbit with its plane normal to z axis.

3. Control

3.1. Sliding Mode Control

Because the manoeuvres required to achieve a hovering state are executed in a dynamical environment that is generally uncertain, an effective implementation of such requires employing control algorithms that are robust against unmodeled perturbations. To this regard, sliding mode control (SMC) is considered to be one of the most effective techniques for controlling dynamical systems with uncertainties [16]. The idea behind SMC is to design a controller capable of maintaining a properly chosen constraint, i.e. a sliding surface, by means of high-frequency control switching. Once the system dynamics is on the sliding surface, it is constrained to remain there, resulting in robust and adaptive control, although it often comes with actuator chattering due to the frequent switch of discontinuous control signal.

3.2. Design of Sliding Surface

Define vectors for state $\boldsymbol{\chi} = [\rho, \theta, z]^T$ and control $\boldsymbol{u} = [\alpha, \delta]^T$. Now the control objective is to force the reduced state $\boldsymbol{\chi}_r = [\rho, z]^T$ to asymptotically track the desired state $\boldsymbol{\chi}_d = [\rho_d, z_d]^T$, regardless of the polar angle θ, by only varying the attitude angles α and δ.

Define tracking error vector as $\boldsymbol{e} = \boldsymbol{\chi}_r - \boldsymbol{\chi}_d$, the sliding surface can be chosen as:

$$\boldsymbol{s} = \dot{\boldsymbol{e}} + \mathbf{k}\boldsymbol{e} \tag{13}$$

where $\mathbf{k}$ is a diagonal positive-definite matrix to be designed.

Then, inspired by the terminal sliding surface used in Ref. [22], a similar non-singular terminal sliding surface is designed as

$$\boldsymbol{\sigma} = \boldsymbol{s} + k_0 \dot{\boldsymbol{s}}^{\frac{p}{q}} \tag{14}$$

where k_0 is a positive constant, p and q are positive odd numbers, holding $1 < p/q < 2$. The application of this terminal sliding surface guarantees the convergence of tracking error within finite time.

3.3. Design of Controller

For the non-affine control system, it is more convenient to choose $\dot{\boldsymbol{u}}$ as the control input instead of $\boldsymbol{u}$. $\dot{\boldsymbol{u}}$ will appear in linear form if Eq. (10) is further differentiated to $\ddot{\boldsymbol{\chi}}$, shown as:

$$\ddot{\boldsymbol{\chi}} = \boldsymbol{h}(\chi_r, \dot{\chi}_r) + \dot{\mathbf{C}}_I^o \mathbf{C}_E^I \boldsymbol{a}_{SRP} + \mathbf{C}_I^o \mathbf{C}_E^I \mathbf{B}(\boldsymbol{u})\dot{\boldsymbol{u}} \tag{15}$$

There are two notable points: firstly, the result of $\mathbf{C}_I^o \mathbf{C}_E^I \mathbf{B}(\boldsymbol{u})\dot{\boldsymbol{u}}$ neglects the second row since θ is not concerned; Secondly, $\boldsymbol{h}$ can be further split as

$$\boldsymbol{h} = \boldsymbol{h_0} + \boldsymbol{d} \tag{16}$$

where $\boldsymbol{h_0}$ is the known part of the derivative of point-mass gravity $-\mu \boldsymbol{r}/r^3$, and $\boldsymbol{d}$ is the unknown part of non-spherical gravity disturbances. Such split takes account the normal case that the non-spherical perturbation of an asteroid is not precisely known until in-situ visit. Recall that in the module of dynamics, a polyhedron gravity field model is used for precise propagation. In addition, assumption is made that $\boldsymbol{d}$ is bounded, holding $\|\boldsymbol{d}\| \leq \boldsymbol{D}$.

After obtaining $\ddot{\boldsymbol{\chi}}$, Eq. (13) is differentiated twice so that, considering Eq. (15), the dynamics of $\boldsymbol{s}$ is obtained as:

$$\ddot{\boldsymbol{s}} = \boldsymbol{h} + \dot{\mathbf{C}}_I^o \mathbf{C}_E^I \boldsymbol{a}_{SRP} + \mathbf{C}_I^o \mathbf{C}_E^I \mathbf{B}(\boldsymbol{u})\dot{\boldsymbol{u}} - \dddot{\boldsymbol{\chi}}_{\boldsymbol{d}} + \mathbf{k}\ddot{\boldsymbol{e}} \tag{17}$$

Next, Eq. (14) is differentiated once so that $\ddot{\boldsymbol{s}}$ appears:

$$\dot{\boldsymbol{\sigma}} = k_0 \frac{p}{q} \mathrm{diag}\left(\dot{\boldsymbol{s}}^{\frac{p}{q}-1}\right)\left(\frac{q}{kp}\dot{\boldsymbol{s}}^{2-\frac{p}{q}} + \ddot{\boldsymbol{s}}\right) \tag{18}$$

If the reaching law to terminal sliding surface is chosen as:

$$\dot{\boldsymbol{\sigma}} = \mathrm{diag}\left(\dot{\boldsymbol{s}}^{\frac{p}{q}-1}\right)\left(-\varepsilon_1 \boldsymbol{\sigma} - \varepsilon_2 \mathrm{sign}(\boldsymbol{\sigma})\right) \tag{19}$$

once the dynamics flow to $\boldsymbol{\sigma} = \mathbf{0}$, $\boldsymbol{s}$ will converge to $\mathbf{0}$ rapidly as well as $\boldsymbol{e}$, where ε_1 and ε_2 are positive parameters to be designed.

Finally, substituting Eq. (17) into Eq. (18) and combining Eq. (18) and (19), the control law can be obtained as:

$$\dot{\boldsymbol{u}} = (\mathbf{C}_I^o \mathbf{C}_E^I \mathbf{B})^{-1} \begin{bmatrix} \dddot{\boldsymbol{\chi}}_d - \boldsymbol{h} - \dot{\mathbf{C}}_I^o \mathbf{C}_E^I \boldsymbol{a}_{SRP} \\ -\mathbf{k}\ddot{\boldsymbol{e}} - \frac{q}{kp}\dot{\boldsymbol{s}}^{2-\frac{p}{q}} - \varepsilon_1 \boldsymbol{\sigma} - \varepsilon_2 \mathrm{sign}(\boldsymbol{\sigma}) \end{bmatrix} \tag{20}$$

3.4. Design of Adaptive Estimation in Controller

The boundary of gravity disturbances $\boldsymbol{d}$ is separately updated by an adaptive estimation law, designed as:

$$\hat{\dot{\boldsymbol{D}}} = \gamma \frac{k_0 p}{q} \mathrm{diag}\left(\dot{\boldsymbol{s}}^{\frac{p}{q}-1}\right)|\boldsymbol{\sigma}| \tag{21}$$

where γ, the updating rate, is a positive number to be designed.

With the adaptive law, the control law of $\dot{\boldsymbol{u}}$ is finalised as:

$$\dot{\boldsymbol{u}} = (\mathbf{C}_I^o \mathbf{C}_E^I \mathbf{B})^{-1} \begin{bmatrix} \dddot{\boldsymbol{\chi}}_d - \boldsymbol{h}_0 - \hat{\boldsymbol{D}} - \dot{\mathbf{C}}_I^o \mathbf{C}_E^I \boldsymbol{a}_{SRP} \\ -\mathbf{k}\ddot{\boldsymbol{e}} - \frac{q}{kp}\dot{\boldsymbol{s}}^{2-\frac{p}{q}} - \varepsilon_1 \boldsymbol{\sigma} - \varepsilon_2 \mathrm{sign}(\boldsymbol{\sigma}) \end{bmatrix} \tag{22}$$

4. Results

4.1. Simulation of Hovering

In this section, the case of hovering on a displaced orbit above Eros is simulated. The physical parameters for simulation are listed in Table 1. The pre-defined parameters in the controller are listed in Table 2.

Choosing the desired hovering orbit as $[\rho_d, z_d]^T = [18{,}40]$ km and the initial conditions as $[\rho, \theta, z]^T = [18.1 \text{ km}, -\pi/2, 39.9 \text{ km}]$ (not on the reference orbit), $[\dot{\rho}, \dot{\theta}, \dot{z}]^T = [-1 \text{ m/s}, -3.3117 \times 10^{-4} \text{ rad/s}, 1 \text{ m/s}]$, the trajectory of solar sail is shown in Fig. 2 where the solar sail is driven to the desired trajectory clockwise. The control history is shown in Fig. 3. Detailed examination to the response curve shows that the cone angle α fluctuated above and below 53 deg with chattering, which is a net result of combating the non-spherical disturbances of the asteroid and inherent SMC characteristic. Fig. 4 is the response to tracking errors, showing that they converge to less than 1 m within 7.8 hours. Despite the polar angle is not controlled, the general pattern of its variation needs to be understood. Fig. 5 shows that time derivative of the polar angle $\dot{\theta}$

(presented in units of asteroid spin rate ω) behaves in near-sinusoidal way. Looking back into Eq. (10) may reveal the reason. At steady state, $\dot{\rho} = 0$ and g_θ is lower in magnitude than f_θ, therefore f_θ dominates the general variation of $\ddot{\theta}$. Furthermore, f_θ contains the trigonometric term of $\boldsymbol{u} = [\alpha, \delta]^T$ with near-constant α at steady state, and thus f_θ changes with δ sinusoidally, leading to a near-sinusoidal $\dot{\theta}$ as a result.

Table 1. Physical parameters for simulation

	Value
Eros Gravitational Constant μ	4.4602×10^4 km^3/s^2
Eros Spin Rate ω	3.3117×10^{-4} rad/s
Eros Heliocentric Distance R	1.6917×10^6 km
Solar Incidence Angle φ	0 deg
Sail Lightness Number β	0.2

Table 2. Parameters in controller

	Value
$\mathbf{k}$	diag(1,1) (s^{-1})
k_0	1×10^6 (km$^{1-p/q}$ / s$^{1-2p/q}$)
p	7
q	5
ε_1	1×10^{-9} (s^{-1})
ε_2	1×10^{-9} (s^{-1})
γ	1

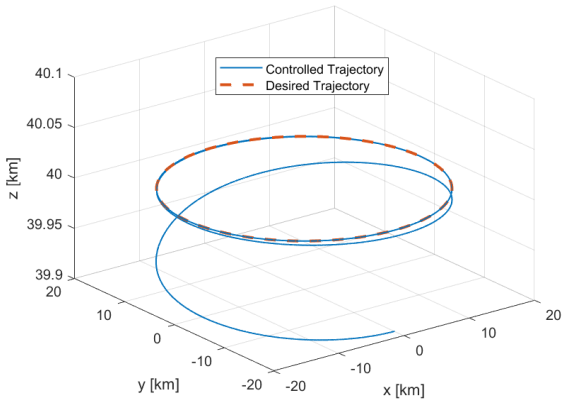

Fig. 2. Controlled trajectory of solar sail.

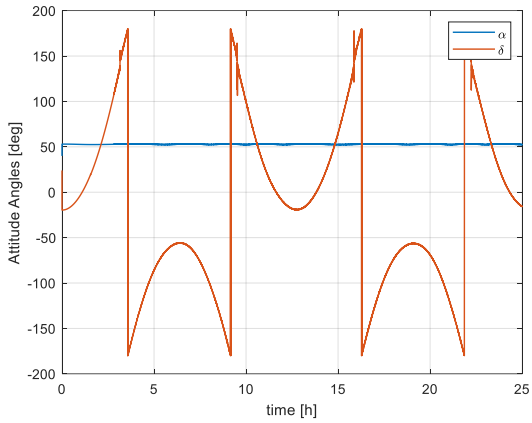

Fig. 3. Time history of control attitude angles.

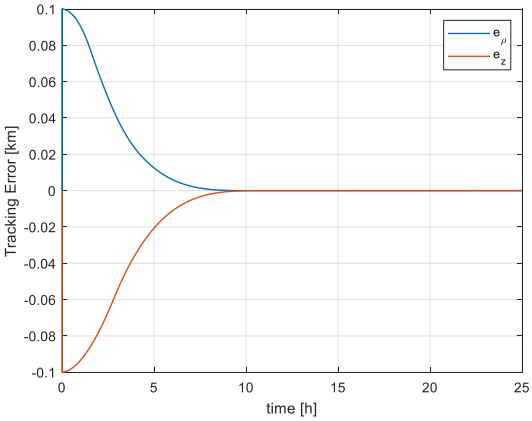

Fig. 4. Response to tracking errors.

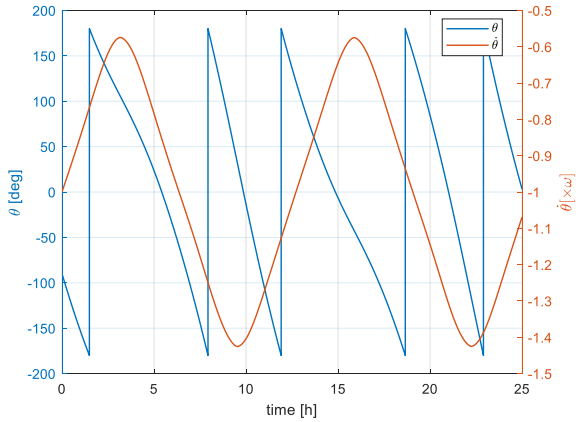

Fig. 5. Polar Angle θ and its time derivative $\dot{\theta}$.

4.2. Robustness

4.2.1. Sail Degradation

Optical degradation of a solar sail is a practical concern because it decreases both the magnitude of SRP

and sail control authority [23]. When degradation happens, the lightness number β decreases, which is equivalent to superpose an equi-magnitude but reverse disturbance onto the controlled SRP acceleration. A scenario is assumed that β is degraded from 0.2 to 0.15 exponentially with 99% attenuation at 15 hours (much faster than real degradation would be). It can be fitted as:

$$\beta(t) = 0.05e^{-t/13500} + 0.15 \qquad (23)$$

With the nominal value of β staying at 0.2, the simulation shows a successful controlled trajectory the same as that in Fig. 2, while the response of cone angle α is different. In Fig. 6, the control of cone angle α in ideal (Section 4.1) and optical degradation (Section 4.2) cases are compared. When optical degradation occurs, the cone angle automatically decreases to compensate the reduction of SRP magnitude and the orbit control is still maintained. This result demonstrates the robustness of the control law to internal disturbances of sail modelling error.

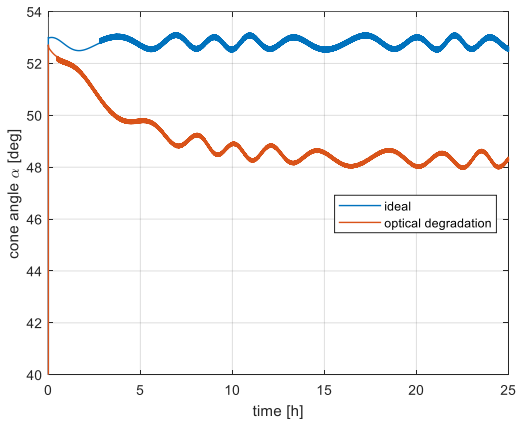

Fig. 6. Control of cone angle in ideal (blue) and optical degradation (red) cases.

4.2.2. *Gravity Field*

Recalling that the simple point-mass gravity is used in the controller design, the robustness to gravity disturbances can be further tested. Now it is assumed that, in the propagation of the dynamics, the real mass of Eros is two times of the nominal value used in the controller. Fig. 7 indicates that the scenario is identified by the control law and cone angle is adjusted down to about 41 deg while it remains around 53 deg with nominal Eros mass in dynamics. The fact that hovering control still works demonstrates that the control law is robust to the unknown external gravity disturbances. It is also worth noting that the control is still robust even without the adaptive estimation law of Eq. (21). Further enlarging the real mass of Eros shows that the robustness of control is increased by introducing the estimation on $\boldsymbol{D}$ (see Eq. (21)): the control without the adaptive estimation breaks down until the real mass increases to 3 times of the nominal value approximately, while with the adaptive estimation it fails with the real mass up to 3.4 times of the nominal value.

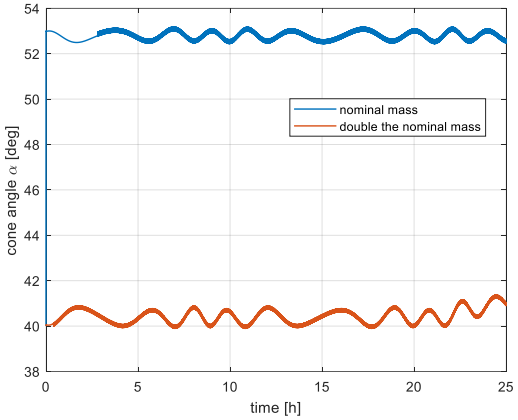

Fig. 7. Control of cone angle in real dynamics with nominal asteroid mass (blue) and double asteroid mass (red).

4.3. *Effect of hovering radius and height*

After the injection manoeuvre, the values of cone angle at steady state are relevant to the polar radius ρ_d and height z_d of the displaced hovering orbit. The cone angles with ρ_d = 18 km, z_d = 30, 40, 50 km are shown in Fig. 8, while those with z_d = 40 km, ρ_d = 10, 18, 24 km are shown in Fig. 9, which demonstrate that a solar sail can achieve hovering in different locations above the asteroid to implement tasks with different requirements without changing any optical properties or lightness number. It can be found that smaller hovering height and radii require smaller cone angles because larger SRP component is needed to counterbalance the gravity in z-axis direction as the solar sail gets closer to the barycentre of the asteroid, as well as to supply larger centripetal force in smaller circular orbits. Moreover, cone angles experience a more intense oscillation as a result of disturbance rejection in the cases of smaller hovering height and larger hovering radii. This is because the effect of perturbation of irregular shape becomes more obvious as the solar sail gets closer to the asteroid in z-axis direction. As the hovering radius becomes smaller, the solar sail undergoes less variation of gravity perturbation in Oxy plane. An extreme case will be the station-keeping above the north pole of the asteroid where planar gravity perturbation keeps constant.

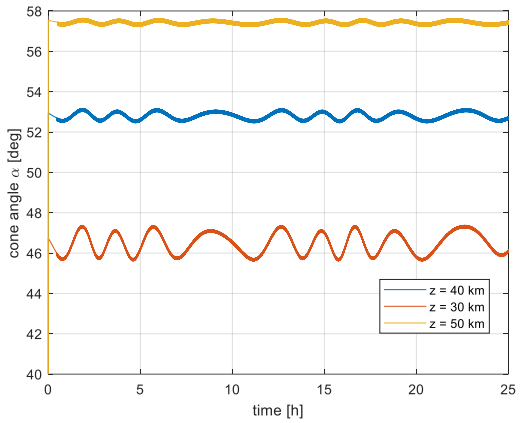

Fig. 8. Cone angle at steady state with ρ_d = 18 km.

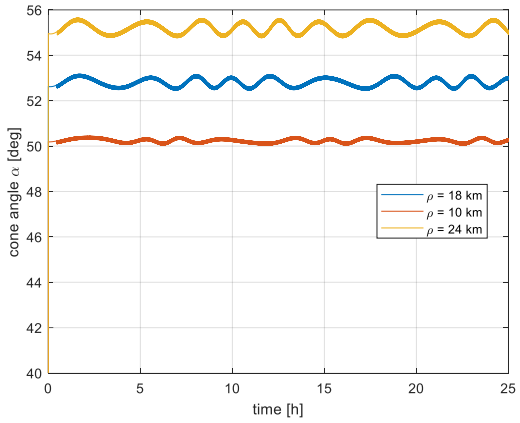

Fig. 9. Cone angle at steady state with z_d = 40 km.

4.4. Effect of Sunlight Incidence Direction

The sunlight incidence angle φ is affected by two elements: heliocentric orbital inclination and obliquity of the ecliptic. Within one orbital period of Eros, φ can vary in a large range. For example, when NEAR Shoemaker was orbiting Eros in 26 June 2000, its rotation axis was perpendicular to the Sun-Eros line ($\varphi = 90$ deg), and 7 months later, it became aligned with Sun-Eros line ($\varphi = 0$ deg) [24]. Simulations with φ = 0, 15, 30, 60, 90 deg are made to study the influence of sunlight incident direction on the hovering control. The results of trajectories and control are presented in Fig. 10. For the cases of φ = 0, 15 deg, the orbit keeping succeeds; when φ grows larger than 30 deg, the displaced orbit fails to be maintained; when φ = 90 deg, the control breaks down in manoeuvre stage. It is obvious that the control is only effective for a set of small values of φ. An explicit reason is that a solar sail can never produce sunward SRP force which is always required by the controller as long as φ is not zero. To this concern, an auxiliary SEP propulsion system may be installed on the sail to complement the missing component towards the Sun, or the solar sail should be driven into other anchor locations during infeasible sunlight incidence period, such as heliocentric solar synchronous orbit.

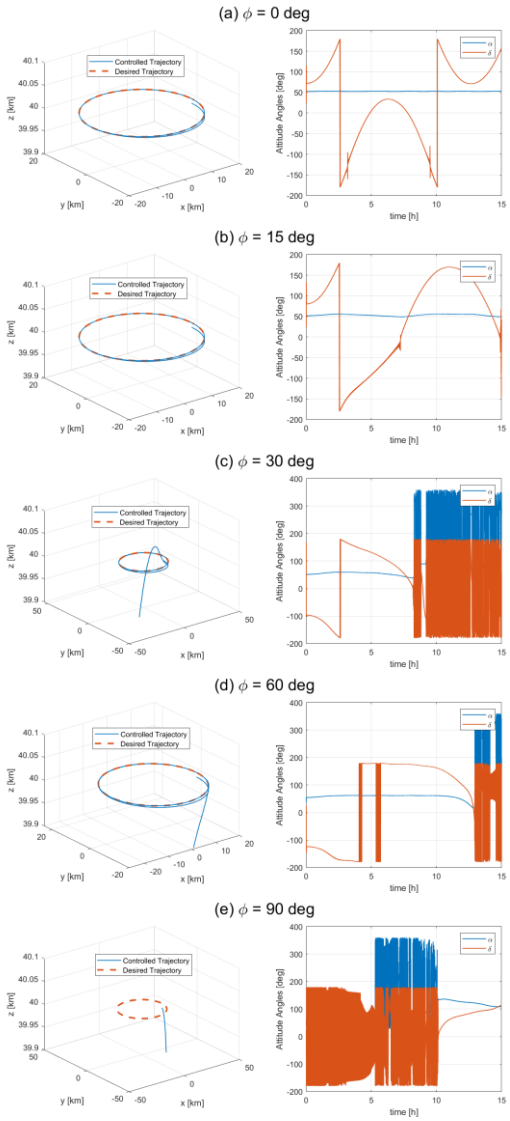

Fig. 10. Trajectories and control of hovering control with sunlight incidence angle (a) φ = 0 deg, (b) φ = 15 deg, (c) φ = 30 deg, (d) φ = 60 deg, (e) φ = 90 deg.

5. Conclusions

In this paper, a hovering orbit controller based on second-order sliding mode theory is designed for solar sail spacecraft on asteroid displaced orbit. Not only does it provide an insight into tackling the problems of underactuated and non-affine control, but also behaves robustly enough to the external unmodelled gravity disturbances and internal imprecise modelling of forces exerted on the sail. Simulation results indicate that smaller hovering radii and height lead to smaller cone

angle. In addition, smaller hovering height and larger radii induce more obvious oscillations in the cone angle. Furthermore, because of the natural shortcoming of solar sailing that it cannot generate sunward force, the controller only works for small sunlight incidence angles. However, a quantitative analysis is lacking in the result analysis. Future work can search feasible ranges of hovering height, radii and sunlight incident direction, as well as improving the quality of the control. The direct observer on gravity disturbance $\boldsymbol{d}$ will be designed instead of its boundary $\boldsymbol{D}$ as follow-up work.

References

[1] Prockter, L., et al., *The NEAR Shoemaker mission to asteroid 433 Eros.* Acta Astronautica, 2002. **51**(1-9): p. 491-500.

[2] Yoshikawa, M., et al., *Sample Return Missions*, in *Sample Return Missions*. 2021, Elsevier. p. 123-146.

[3] Zeng, X., S. Gong, and J. Li, *Fast solar sail rendezvous mission to near Earth asteroids.* Acta Astronautica, 2014. **105**(1): p. 40-56.

[4] Dachwald, B., W. Seboldt, and L. Richter, *Multiple rendezvous and sample return missions to near-Earth objects using solar sailcraft.* Acta Astronautica, 2006. **59**(8-11): p. 768-776.

[5] Peloni, A. and M. Ceriotti, *Solar-Sail Trajectory Design for a Multiple Near-Earth-Asteroid Rendezvous Mission.* Journal of Guidance, Control, and Dynamics 2016. **39(12)**.

[6] Guelman, M.M., *Closed-loop control for global coverage and equatorial hovering about an asteroid.* Acta Astronautica, 2017. **137**: p. 353-361.

[7] Yang, H., X. Bai, and H. Baoyin, *Finite-time control for asteroid hovering and landing via terminal sliding-mode guidance.* Acta Astronautica, 2017. **132**: p. 78-89.

[8] Moore, I., M. Ceriotti, and C.R. McInnes, *Station-keeping for a solar sail during lander/probe deployment using feedback control.* Acta Astronautica, 2022. **201**: p. 182-197.

[9] Scheeres, D.J., *Close proximity dynamics and control about asteroids*, in *American Control Conference*. 2014: Portland, Oregon, US. p. 1584-1598.

[10] Biggs, J.D. and C.R. McInnes, *Time-Delayed Feedback Control in Astrodynamics.* Journal of Guidance, Control, and Dynamics, 2009. **32**(6): p. 1804-1811.

[11] Farrés, A., S. Soldini, and Y. Tsuda, *JAXA's Trojan Asteroids Mission Trajectory Design of the Solar Power Sail and its Lander*, in *The 4th International Symposium on Solar Sailing*. 2017: Kyoto, Japan.

[12] Farrés, A., et al., *Periodic Motion for an Imperfect Solar Sail Near an Asteroid*, in *The 3rd International Symposium on Solar Sailing*. 2014: Glasgow, UK.

[13] Farrés, A., À. Jorba, and J. Mondelo, *Orbital Dynamics for a Non-perfectly Reflective Solar Sail Close to an Asteroid*, in *The 2nd IAA Conference on Dynamics and Control of Space Systems*. 2014: Rome, Italy.

[14] Zeng, X., et al., *Solar Sail Body-Fixed Hovering over Elongated Asteroids.* Journal of Guidance, Control, and Dynamics, 2016. **39**(6): p. 1223-1231.

[15] Moore, I. and M. Ceriotti, *Solar sails for perturbation relief: Application to asteroids.* Advances in Space Research, 2021. **67**(9): p. 3027-3044.

[16] Furfaro, R., *Hovering in Asteroid Dynamical Environments Using Higher-Order Sliding Control.* Journal of Guidance, Control, and Dynamics, 2015. **38**: p. 263-279.

[17] Batista Negri, R. and A.F.B.A. Prado, *Autonomous and Robust Orbit-Keeping for Small-Body Missions.* Journal of Guidance, Control, and Dynamics, 2022. **45**(3): p. 587-598.

[18] Werner, R.A. and D.J. Scheeres, *Exterior Gravitation of a Polyhedron Derived and Compared with Harmonic and Mascon Gravitation Representations of Asteroid 4769 Castalia.* Celestial Mechanics and Dynamical Astronomy, 1997. **65**: p. 313-344.

[19] McInnes, C., *Solar Sailing: Technology, Dynamics and Mission Applications*. 1999, Chichester, England, UK: Springer Praxis.

[20] McInnes, C. and J. Simmons, *Solar Sail Halo Orbits II: Geocentric Case.* Journal of Spacecraft and Rockets, 1992. **29**: p. 472-479.

[21] Bookless, J. and C.R. McInnes, *Dynamics and Control of Displaced Periodic Orbits Using Solar Sail Propulsion.* Journal of Guidance, Control, and Dynamics, 2006. **29**: p. 527-537.

[22] Chen, Y., et al. *Adaptive Second-order Sliding Mode Station-keeping Control for Solar Sail Spacecraft on Displaced Orbit*. in *The 38th Chinese Control Conference*. 2019. Guangzhou, China.

[23] Dachwald, B., W. Seboldt, and M.e.a. Macdonald, *Potential Solar Sail Degradation Effects on Trajectory and Attitude Control*, in *AIAA Guidance, Navigation and Control Conference and Exhibit*. 2005: San Francisco, California.

[24] Farquhar, R., J. Kawaguchi, and C.T.e.a. Russell, *Spacecraft Exploration of Asteroids: The 2001 Perspective*, in *Asteroids III*, W.F. Bottke Jr., et al., Editors. 2002, University of Arizona Press. p. 367-376.